# Spectral splitting and wave-function scaling in quasicrystalline and hierarchical structures

Qian Niu
*Department of Physics, University of California, Santa Barbara, California 93106*
*and Department of Physics, University of Texas, Austin, Texas 78712**

Franco Nori
*Department of Physics, University of Michigan, Ann Arbor, Michigan 48109-1120*
(Received 8 August 1990)

We give a comprehensive presentation of a renormalization-group theory for the study of a set of one-dimensional Schrödinger equations on quasicrystalline and hierarchical structures. Particular attention is focused on the spectral clustering and wave-function scaling properties. New results are given on (i) a general characterization of the wave functions, (ii) the scaling of the localized edge states, and (iii) a hierarchical-lattice implementation of the renormalization group.

## I. INTRODUCTION

Pioneering work on aperiodic GaAs-AlAs superlattices,[1-5] the discovery of the quasicrystalline phases,[6] and the fabrication of other low-dimensional quasiperiodic structures[7-9] has generated a renewed interest in the study of electronic properties of one-dimensional (1D) quasicrystalline (QC) Schrödinger equations. For excellent surveys, we refer the reader to Refs. 10 and 11.

The spectral and wave-function properties of these systems have been extensively studied by using several approaches.[12-40] While most work has been done numerically, analytical approaches based on trace maps[15-30] and real-space decimation techniques[31-36] have played the central role in our understanding of such systems. In 1986 we proposed a renormalization-group (RG) theory based on a decimation scheme derived from degenerate perturbation calculations.[12] While it is exact only in a certain limit, it offers us an intuitive and coherent picture about the physics of the system. Besides, it gives a simple analytical framework, in which extensive analysis of the spectral and wave-function structures can be carried out. Here we give a more detailed account of our work. New results will be presented on (i) a general characterization of the wave functions, (ii) the scaling of the localized edge states, and (iii) a hierarchical-lattice implementation of the RG.

The main character of our RG scheme may be summarized as follows. The original system is decoupled into a few subsystems, each of which corresponds to the original system with renormalized coupling parameters and length scales. The recursion relation for each branch is explicitly given, and it only depends on the type of the branch. The subsystems then branch into sub-subsystems in a similar fashion, and so on.

More specifically, this RG scheme[12] is a recursive block diagonalization of the Hamiltonian matrix representing the original system. The diagonal blocks are the subsystems. As a block is further diagonalized into subblocks, the corresponding subsystem is decomposed in sub-subsystems. At the end of the RG flow, we obtain the individual energy levels and wave functions. Their properties can be inferred from the structure of the RG flow. In particular, the branching character of the RG scheme implies a hierarchical structure of the spectrum and wave functions.

Our RG theory has been applied to an analysis of the roughening of two-dimensional quasicrystal interfaces by Garg.[13] In this work he computed the leading low-temperature behavior of the roughness exponent. In an appendix of his article, he rederived, in slightly different terms, some basic results of the RG theory.

The RG theory presented here has also provided a simple analytic basis for a global scaling analysis of the spectrum by Zheng.[14] His result compares qualitatively well with the numerical result of Ref. 15 and is exact in the limit of $|T_w/T_s| \ll 1$, where $T_w$ ($T_s$) corresponds to the weak (strong) hopping amplitudes of the chain.

Finally, we should mention that our RG theory can be applied to other aperiodic lattices with hierarchical couplings.[41-44]

This work is organized as follows. In Sec. II we introduce the basic ideas by studying a chain with hierarchical couplings. In Sec. III we implement the real-space decimation approach for the quasicrystalline lattice. The branching patterns of the electronic spectra are analyzed in more detail in Sec. IV. The behavior of the wave functions is considered in Sec. V for the generic case and in Sec. VI for the localized gap (surface) states.[37] Finally, in Sec. VII we summarize the basic results, discuss the merits and shortcomings of the theory, and point out some conceivable applications for the future. Appendixes A and B are devoted to the mathematical details of the calculation of the renormalized coupling parameters.

## II. RG FOR A HIERARCHICAL MODEL

Although our real-space decimation approach was originally introduced through studying a well-known aperiodic system, a 1D quasicrystal or Fibonacci chain, the idea can be applied to many other systems. One such example is the class of tight-binding Hamiltonians on structures with hopping amplitudes arranged in a hierarchical manner. This kind of structure has been ex-

 

tensively studied.[41-44] In fact, the basic idea of the RG theory can be most clearly exposed through the hierarchical model. It is for this reason that we shall now consider this model before the Fibonacci-chain case.

Suppose we have a one-dimensional chain of sites on which a quantum particle lives. Assume that the site energies are all equal to $E_0$, and that the hopping amplitudes are nonzero only for nearest neighbors. The hierarchical structure is then built up by a spatial distribution of the hopping amplitudes. The following description gives a simple example. First, for every other one of all the nearest neighbors, we take $T_1$ as the hopping amplitude. Next, for every other one of the remaining nearest neighbors, we take $T_2$ as the hopping amplitude. Then, for every other one of the nearest neighbors unspecified before, we take $T_3$. The process goes on until all the nearest neighbors are specified. Therefore, a fraction $2^{-n}$ of the nearest neighbors have $T_n$ as the hopping amplitude. We wish to consider the case that, for each $n$, $|T_{n+1}/T_n|$ is much smaller than 1. The hierarchical structure of the chain is then quite obvious.[41-44] The sites are grouped into pairs by $T_1$, and the pairs are grouped into superpairs by $T_2$, and so on. This is illustrated schematically in the top chain of Fig. 1. It is convenient to call a set of sites grouped together by $\{T_1, T_2, \ldots, T_n\}$ as an $n$th-order "molecule". Accordingly, the sites may be called as molecules of zeroth order, and the infinite lattice as a molecule of infinite order. Thus an $n$th-order molecule contains two neighboring $(n-1)$th-order molecules coupled by $T_n$, each of which contains two $(n-2)$th-order molecules coupled by $T_{n-1}$, and so on.

At the first step of our RG, we diagonalize the tight-binding Hamiltonian up to terms of order $T_1$. This is achieved by writing the Hamiltonian matrix in the basis

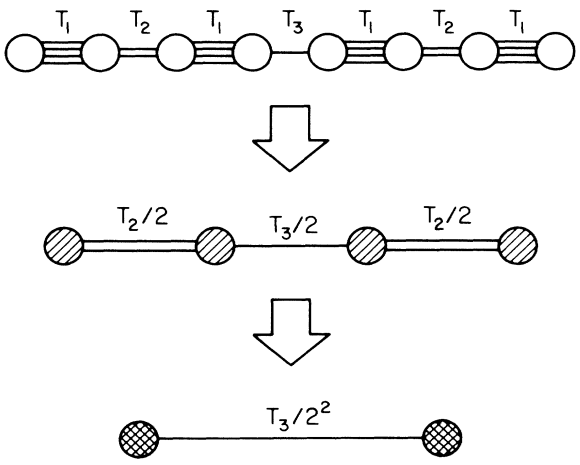


FIG. 1. Schematic representation of the renormalized group (RG) decimation procedure for a lattice with hierarchical couplings (top chain). The hopping energies satisfy $T_1 \gg T_2 \gg T_3$. The renormalized chain, shown in the center, consists of the bonding states of the strongly coupled pairs of sites in the original chain. The effective couplings in the new chain are indicated. An identical procedure produces the renormalized chain shown in (c).

of the bonding and antibonding states of the first-order molecules. Specifically, if $|1\rangle$ and $|2\rangle$ are the basis states of the sites of a first-order molecule, then the bonding and antibonding states of the molecule are given, respectively, by

$$\frac{1}{\sqrt{2}}(|1\rangle+|2\rangle)\,, \tag{2.1}$$

and

$$\frac{1}{\sqrt{2}}(|1\rangle-|2\rangle)\,. \tag{2.2}$$

To be more specific for later reference, we assume that site 2 is on the right of site 1. The resultant spectrum then consists of two infinitely degenerate levels at $E=E_0\pm T_1$, where the plus sign is for the bonding states, and the minus sign for the antibonding states.

When the higher-order bonds $(T_2, T_3, \ldots)$ are taken into account, these molecular states are coupled together. However, the dominant effect is the resonant coupling of the states with the same energy. We wish to construct an effective Hamiltonian for each of the degenerate levels. This can be done according to the formalism described in Appendixes A and B, where we take $H_0$ as the part of the Hamiltonian containing all the first-order bonds $T_1$, and $H_1$ as the remaining part. Let us focus our attention on the bonding level $E_0+T_1$ first. As an approximation, the effective hopping amplitudes will be carried out to the leading term in the expansion for each of the nearest neighbors of the molecules only, and the energy shifts will be ignored. The resultant effective hopping amplitudes $\{T_1', T_2', \ldots\}$ are then given by

$$T_n' = \tfrac{1}{2}T_{n+1}\,, \tag{2.3}$$

where $T_n'$ is for two nearest-neighboring molecules originally coupled by $T_{n+1}$. Incidentally, the above formula is actually correct to second order in $H_1$. The ignored energy shifts are of order $T_2^2/T_1$ or smaller. We have therefore obtained a renormalized lattice described by the new-site energy

$$E_0' = E_0 + T_1\,, \tag{2.4}$$

and the set of new coupling constants $\{T_1', T_2', \ldots\}$. The sites of the renormalized lattice are the first-order molecules of the original lattice, and the new-site states are the bonding molecular states of the original lattice. The renormalized lattice has a similar hierarchical structure as before, with the new sites grouped into molecules of various orders by the set of new hopping amplitudes. These hopping amplitudes satisfy $|T_{n+1}'/T_n'| \ll 1$ as before. See Fig. 1 for an illustration.

For the antibonding level $E_0-T_1$, we repeat the above procedure. The renormalized lattice for this level is then described by a site energy $E_0'=E_0-T_1$ and by a set of effective coupling constants $\{T_1', T_2', \ldots\}$ given by

$$T_n' = -\tfrac{1}{2}T_{n+1}\,. \tag{2.5}$$

This completes the first step of our RG.

The subsequent steps go on in a similar fashion. Sup-

pose we have obtained, after the $m$th step, a renormalized lattice $L_m$, with a site energy $E_0^{(m)}$ and a set of nearest-neighbor hopping amplitudes $\{T_1^{(m)}, T_2^{(m)}, \ldots\}$ with $|T_{n+1}^{(m)}/T_n^{(m)}| \ll 1$; then it can be renormalized again to give rise to two new effective lattices. As was done in the first step, the Hamiltonian of $L_m$ is first diagonalized to the order of $T_1^{(m)}$, by using the bonding and antibonding states of the first-order molecules of $L_m$. The two degenerate levels so obtained are perturbed by the high-order hopping amplitudes $\{T_n^{(m)}, n>1\}$, but again the dominant effect is taken into account by the leading terms of the degenerate perturbation expansion. With a similar approximation as in the first step, an effective Hamiltonian is constructed for each of the degenerate levels. Thus, for the bonding level, we have

$$E_0^{(m+1)} = E_0^{(m)} + T_1^{(m)} , \tag{2.6a}$$

$$T_n^{(m+1)} = \tfrac{1}{2} T_{n+1}^{(m)} , \quad n = 1,2,\ldots . \tag{2.6b}$$

The new renormalized lattice for this level then consists of the bonding molecules of $L_m$ as its sites (or site states). And because $|T_{n+1}^{(m+1)}/T_n^{(m+1)}| \ll 1$ is satisfied for each $n$ as before, the sites of the new lattice are grouped into a hierarchical structure of molecules of various orders by the set of hopping amplitudes $\{T_1^{(m+1)}, T_2^{(m+1)}, \ldots\}$. For the antibonding level, we have

$$E_0^{(m+1)} = E_0^{(m)} - T_1^{(m)} , \tag{2.7a}$$

$$T_n^{(m+1)} = -\tfrac{1}{2} T_{n+1}^{(m)} , \quad n = 1,2,\ldots . \tag{2.7b}$$

Having described the general procedure of the RG, we now introduce a scheme to specify the renormalized lattices. There are $2^m$ number of renormalized lattices produced in the $m$th step of the RG. Each of them can be conveniently specified by a symbolic string $p_1 p_2 \cdots p_m$, where each $p$ is either $b$ or $a$ (meaning "bonding" or "antibonding"), depending on how the lattice comes from the renormalization procedure. Specifically, if this lattice comes from the "bonding" level in the $k$th step ($k = 1,2,\ldots,m$), then $p_k = b$; otherwise, $p_k = a$. In this way each renormalized lattice has a proper name given by its symbolic string, and its heritage can be read off from its name. The length of the "name string" tells the generation of the lattice. Also, from the name string, the character of the basis state (in terms of the site states of the original lattice) as well as the location and width of its spectrum can be specified.

From the structure of the RG, it is easy to see how the spectrum of the ultrametric model looks. First, the spectrum is centered about $E_0$ and has a total span of about $2(T_1)$. Second, the spectrum consists of two clusters located around $E_0 \pm T_1$, each with a span of about $2|T_1'| = |T_2|$, corresponding to the renormalized lattices from the first step of the RG. Third, each of the two clusters again consists of two subclusters, with their approximate locations and spans given by

$$E_0^{(2)} = E_0' \pm T_1' = E_0 \pm T_1 \pm \tfrac{1}{2} T_2 , \tag{2.8}$$

and by

$$2|T_1^{(2)}| = |T_2'| = \tfrac{1}{2}|T_3| , \tag{2.9}$$

respectively. These correspond to the renormalized lattices from the second step of the RG. The bifurcation goes on indefinitely. In general, corresponding to the renormalized lattices of the $m$th step of the RG, there are $2^m$ number of small clusters, located around

$$E_0 \pm T_1 \pm \frac{T_2}{2} \pm \cdots \pm \frac{T_m}{2^{m-1}} , \tag{2.10}$$

each with a span of about $|T_{m+1}|/2^m$.

If we had chosen the truncation

$$T_{m+k} = T_{m+1} , \quad k = 2,3,\ldots , \tag{2.11}$$

then, after the $m$th step of the renormalization, we would have obtained $2^m$ chains, each of which have nearest-neighbor couplings given by $(-1)^{n_a} T_{m+1}/2^m$, where $n_a$ is the number of antibonding branches in the $m$ steps of the renormalization. Since each chain gives rise to a bandwidth of $4T_{m+1}/2^m$, the total bandwidth is given by

$$W_m = 4T_{m+1} . \tag{2.12}$$

This result is, in fact, exact according to Ref. 43.

## III. RG FOR A QUASICRYSTALLINE STRUCTURE

### A. Hamiltonian

A one-dimensional version of a quasicrystal, also known as a Fibonacci lattice, can be obtained by projecting a subset of the vertices of a two-dimensional square lattice onto a line with a slope equal to the golden mean $\tau = 2\cos(\pi/5) = (1+\sqrt{5})/2$. The distance between adjacent points in this lattice can only have two values, which will be denoted by $L$ and $S$. The exact Fibonacci sequence $S_\infty$ of $L$'s and $S$'s can also be obtained without using the projection method, but recursively as $S_{m+1} = \{S_{m-1}, S_m\}$, with $S_0 = \{S\}$ and $S_1 = \{L\}$. An alternative method of constructing the Fibonacci sequence is to use the "inflation" transformation $S \to L$, $L \to LS$. This transformation was introduced well before the discovery of quasicrystals, in 1202, by Leonardo da Pisa related to his research on population growth models among mating rabbits. Throughout this paper we will use the terms quasicrystal and quasiperiodic (QP) in order to denote this kind of aperiodic ordering.

We will concentrate our attention on the tight-binding model defined by the eigenvalue problem

$$t_{n,n+1}\psi_{n+1} + t_{n,n-1}\psi_{n-1} + \epsilon_n \psi_n = E\psi_n , \tag{3.1}$$

where $\epsilon_n$ and $\psi_n$ are, respectively, the site energy and probability amplitude at the $n$th site, while $t_{n,n+1} = \langle \psi_n | H | \psi_{n+1} \rangle = t_{n+1,n} \equiv T_n$ is the hopping transition amplitude associated with the bond between sites $n$ and $n+1$. Three cases will be considered. In case $A$ the site energies $\epsilon_n$ are equal to a constant (which will be absorbed into the eigenenergy $E$), and the bonds take two

values $T_s$ (strong) and $T_w$ (weak), arranged in a Fibonacci sequence. This sequence is generated by repeated applications of the (concurrent) substitution rule $T_w \to T_w T_s$ and $T_s \to T_w$, starting from the initial sequence $S_1 = T_w$. Therefore, $S_2 = T_w T_s$, $S_3 = T_w T_s T_w$, $S_4 = T_w T_s T_w T_w T_s$, and so on. Case $B$ is the same as $A$, but with the interchange $T_w \rightleftarrows T_s$, so that the strong bonds are more numerous than the weak ones. In case $C$ all the bonds are equal to a constant $T_n = T$, but the site energies take two values $V_1$ and $V_2$, arranged in a Fibonacci sequence. The corresponding energy spectra for models $A$, $B$, and $C$ are shown in Figs. 2(a), 2(b), and 2(c), respectively, while their band-splitting structures are presented, in a schematic way, in Figs. 3(a), 3(b), and 3(c).

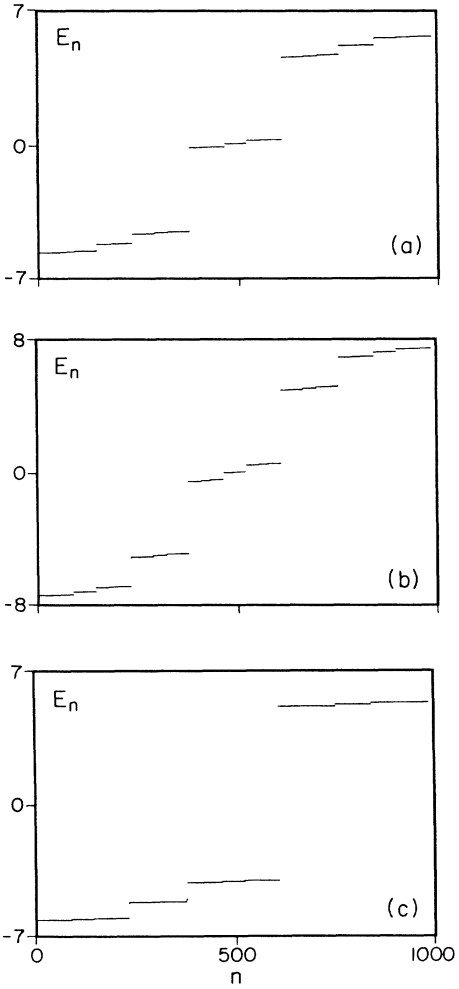


FIG. 2. Energy spectrum for a tight-binding model on a quasicrystalline chain. The chain has 987 sites and fixed-end boundary conditions; $n$ labels the eigenstate with energy $E_n$. The eigenenergies are plotted from left to right in increasing order. (a) Case $A$, Fibonacci sequence of two hopping transition amplitudes with $T_w = 1$, $T_s = 5$, with $T_w$ more numerous. (b) Case $B$, same as before, but now with $T_s$ more numerous. (c) Case $C$, QP sequence of two on-site energies $V_1 = -5$ and $V_2 = +5$, and uniform hopping amplitude $T = 1$.

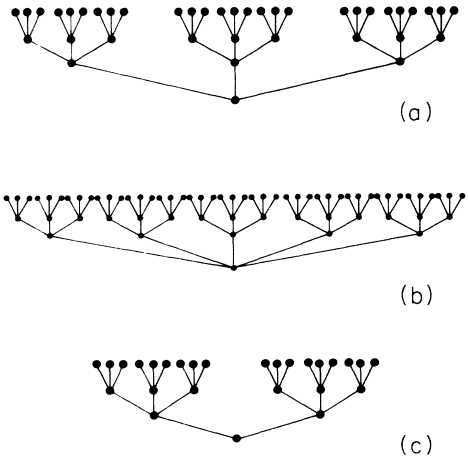


FIG. 3. Spectral-splitting pattern for the energy spectra shown in Fig. 2. (a), (b), and (c) in this figure correspond, respectively, to the (a), (b), and (c) spectra of Fig. 2, and to models $A$, $B$, and $C$. Thus the off-diagonal models $A$ and $B$ have three and five main clusters of states, respectively; while the diagonal QC case has two main clusters. Every main cluster is composed of three subclusters, each of these has three sub-subclusters, and so on.

### B. Summary of the RG analysis of the canonical case $A$

The basic idea of our RG theory[12] is summarized here for the canonical case $A$. It turns out that cases $B$ and $C$ reduce to case $A$ after one step of renormalization. We assume $|T_w/T_s| \ll 1$. In the first step of the RG, we diagonalize the strong bonds. If the weak bonds are ignored, then the spectrum will consist of three degenerate levels, corresponding to states on the isolated sites (atoms), and the bonding and antibonding states (molecules) on the pairs of sites originally connected by the strong bonds. These levels are separated by the energy $|T_s|$, which is, by assumption, much larger than the ignored weak bonds. When the leading corrections of the weak bonds are taken into account, the different states in a degenerate level are connected, but the states belonging to different levels are decoupled. The result is three independent sublattices: (1) bonding molecular chain, (2) atomic chain, and (3) antibonding chain. They have renormalized nearest-neighbor bonds

$$\left\{\frac{T_w^2}{2T_s}, \frac{T_w}{2}\right\}, \quad \left\{\frac{T_w^3}{T_s^2}, \frac{-T_w^2}{T_s}\right\}, \quad \left\{\frac{T_w^2}{2T_s}, \frac{-T_w}{2}\right\}, \tag{3.2}$$

respectively, all arranged in a Fibonacci sequence as $\{T_w, T_s\}$ was in the original lattice. In the subsequent steps of the RG, each of the sublattices is renormalized again into three sub-sublattices, and so on.

A direct consequence of this RG analysis is that the spectrum should have a hierarchical pattern: three major clusters, each of which is trifurcated into three subclusters, and so on. The middle subclusters correspond to the atomic sublattices, and they are narrower by a factor of $|T_w/T_s|$ than the side subclusters sharing the same

parent cluster. The relative spectral weights of the three subclusters from a given parent cluster is

$$\left[\frac{1}{\tau^2},\frac{1}{\tau^3},\frac{1}{\tau^2}\right], \tag{3.3}$$

as can be obtained by counting the relative number of sites involved in a sublattice.

After this summary we consider in detail the three cases described in Sec. III A.

## IV. BRANCHING PATTERNS OF THE ELECTRONIC SPECTRA

### A. Case *A*

Figure 2(a) is a typical plot of the energy spectrum for this case. One of the goals of our RG, as described below, is to explain the trifurcating pattern exhibited in the spectrum.

In the absence of the weak bonds ($T_w=0$), the Fibonacci lattice is broken into isolated sites (atoms) and double sites (molecules). The spectrum then consists of three infinitely degenerate levels: $E=0$ for the atomic states and $E=\pm T_s$ for the bonding and antibonding molecular states. As we take the weak bonds into account, these states are coupled together. However, the dominant effect is the resonant coupling among the states of the same energy.

In the following we will only keep the first few terms in Eq. (A7), just to couple the states in a given level together. Also, energy shifts (which are absent for the $E=0$ level) of the same order as the renormalized weak bond are neglected in order to simplify the description of our RG, although they can be included in all steps of the renormalization.

For the level $E=0$, the renormalized lattice consists of the atomic sites in the original lattice. These sites are connected by the effective bonds $-T_w^2/T_s$ and $T_w^3/T_s^2$. The former is for pairs of atoms separated by one molecule, and the latter is for those pairs of atoms separated by two neighboring molecules. These bonds are arranged in a Fibonacci sequence, and so the structure of the new lattice is the same as its mother lattice (see Fig. 4).

For the level $E=T_s$, the basic units of the renormalized lattice are the bonding molecular states

$$\frac{1}{\sqrt{2}}(|i\rangle+|i+1\rangle), \tag{4.1}$$

where $\{|i\rangle, |i+1\rangle\}$ are the pairs of strongly coupled sites in the original lattice. These units are connected by the effective bonds $T_w/2$ and $T_w^2/(2T_s)$. The former is between the bonding states of neighboring molecules in the original lattice, while the latter is for the bonding states of molecules mediated by an atomic site. Again, the arrangement of the bonds is a Fibonacci sequence, giving the new lattice the same structure as the original one (see Fig. 5).

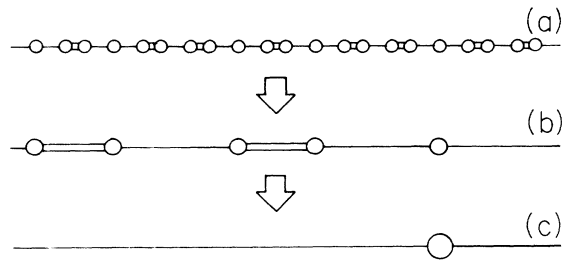


FIG. 4. Schematic representation of the decimation procedure for the central subclusters of the energy spectrum of the off-diagonal Fibonacci lattice, case *A*. This decimation procedure favors the atomic sites. The double (single) lines denote the strong (weak) effective bonds.

Finally, for the level $E=-T_s$, we have a new lattice of antibonding molecules:

$$\frac{1}{\sqrt{2}}(|i\rangle-|i+1\rangle), \tag{4.2}$$

where $\{|i\rangle, |i+1\rangle\}$ are again the pairs of strongly coupled sites in the original lattice. The new effective bonds are $-T_w/2$ and $T_w^2/(2T_s)$ arranged in a Fibonacci sequence. This completes the first step of our RG analysis.

In the second step of our RG analysis, we first remove the weaker bonds in the new lattices obtained in the first step. We are then left with the isolated units (superatoms), and bonding and antibonding double units (supermolecules). The three levels $E=0$ and $\pm T_s$ are then each split into three sublevels. For each of these sublevels we can construct a Fibonacci lattice, using the method of resonant coupling. This decimation procedure is schematically represented in Figs. 4 and 5.

This procedure continues on and on, and eventually we obtain a spectral pattern of three main clusters ("bands"), each of which consists of three subclusters (subbands), and so on. In general, the middle cluster (or subcluster) is narrower than the side clusters by a ratio of order $|T_w/T_s|$. Also, the number of states in the central cluster is $1/\tau$ times that in a side cluster, according to (3.3). This explains the trifurcating structure of the spectrum numerically observed by many authors. If the number of

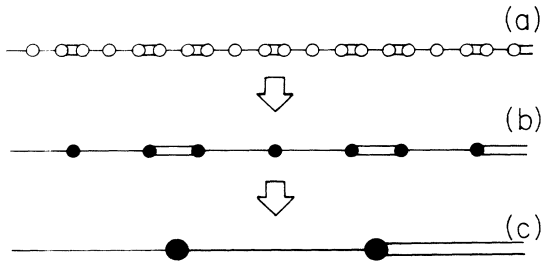


FIG. 5. Decimation procedure favoring the bonding molecular states. The double (single) lines denote the strong (weak) effective bonds. The sites in chain (b) correspond to the bonding states in chain (a). Similarly, the sites in chain (c) correspond to the bonding states in chain (b). This procedure works also for the antibonding states.

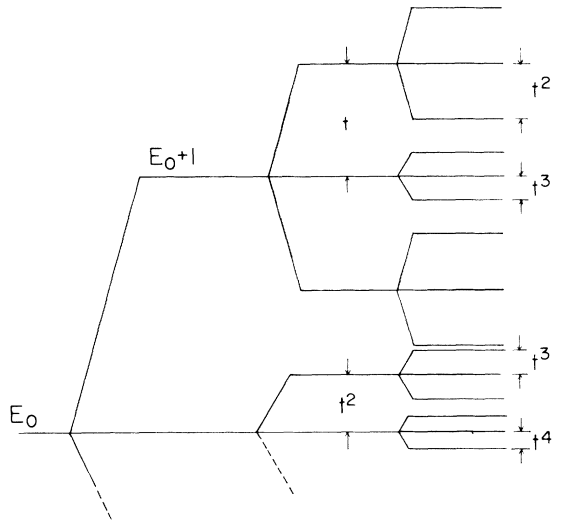


FIG. 6. Level-splitting pattern for the off-diagonal QP case $A$ corresponding to the energy spectra in Figs. 2(a) and 3(a), and the decimation procedures in Figs. 4 and 5. The first bonding and antibonding energy levels have an energy splitting of the order of $t<1$, while the central level splits as $\sim t^2$. The next step produces energy-level splittings as indicated. Note that the side (either top or bottom) clusters are wider than the corresponding central cluster.

states in a cluster is a Fibonacci number $F_n$, then the corresponding three subclusters will have the following number of states: $F_{n-2}$, $F_{n-3}$, and $F_{n-2}$ [see Figs. 2(a) and 6].

It must be emphasized that our RG approach is only exact in the limit of $|T_w/T_s|\ll 1$ [or $|T/(V_1-V_2)|\ll 1$ in case $C$, to be studied later]. However, as can be verified numerically, even $|T_w/T_s|=0.5$ can be regarded as $\ll 1$, for the purpose of giving qualitative predictions. When $|T_w/T_s|\leq 0.2$, predictions about the spans of the clusters become very accurate.

### B. Case *B*

We now consider the off-diagonal case $B$. Figure 7(a) shows the QP sequence of weak ($T_w\equiv t<1$) and strong ($T_s=1$) bonds. The weak bonds have not been drawn, but their locations are indicated by their strength $t$, while the strong bonds are indicated with single lines. The energy levels corresponding to the strongly coupled three-site clusters (triatomic molecules) $\{|i\rangle,|i+1\rangle,|i+2\rangle\}$ are $E=0,\pm\sqrt{2}$, with wave functions, respectively, given by

$$\frac{1}{\sqrt{2}}(|i\rangle-|i+2\rangle)\ , \tag{4.3}$$

$$\tfrac{1}{2}(|i\rangle\pm\sqrt{2}|i+1\rangle+|i+2\rangle)\ , \tag{4.4}$$

while for the dimers (diatomic molecules) $\{|k\rangle,|k+1\rangle\}$, $E=\pm 1$, with wave functions given by

$$\frac{1}{\sqrt{2}}(|k\rangle\pm|k+1\rangle)\ . \tag{4.5}$$

Therefore, when $t=0$ we have five infinitely degenerate levels in the system as is illustrated in Fig. 8.

Because of the energy gaps between the five degenerate levels, the coupling among them due to the weak bonds is negligible for $t\ll 1$. However, the weak bonds will play an important role in splitting each of the degenerate levels. Let us focus our attention on the levels $E=\pm\sqrt{2}$. The constituent states are the bonding states of the triatomic molecules. These states are schematically shown as rectangles in Fig. 7(b). There are two types of couplings among them: the direct ones, $T_s'=t/4$, and those through the dimers, $T_w'=t^2/4$. One can check explicitly that the distribution of these two types of bonds form a Fibonacci sequence, with the weak ones more numerous than the strong ones. This is exactly case $A$, studied in the last subsection.

A careful study of the other degenerate levels shows that they are all equivalent to Fibonacci chains of case $A$, with the pairs of coupling parameters listed in Table I.

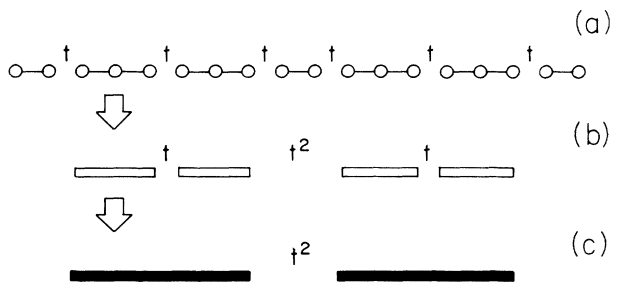


FIG. 7. Decimation procedure favoring the states in the edge clusters $E=\pm\sqrt{2}$ of the spectrum in case $B$. In chain (a) the hopping elements within the indicated groups are 1, and those between the groups are $t<1$. The open rectangles in (b) represent the bonding states of the triatomic molecules in (a), and $t,t^2$ are the new coupling energies between them. The strongly coupled units in (b) form the units in (c).

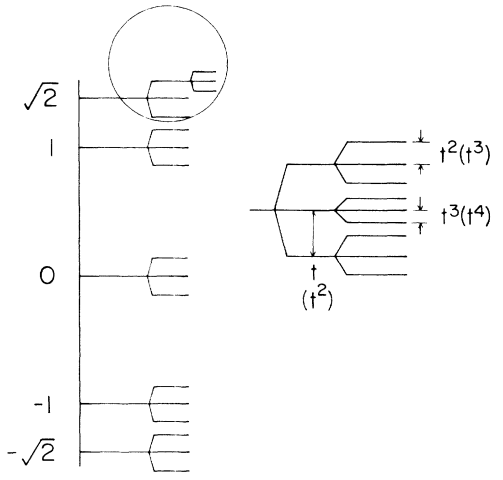


FIG. 8. Energy-level-splitting diagram for the off-diagonal case $B$. The energy levels group in five clusters, each one of them trifurcating indefinitely. The levels enclosed by the circle have been magnified and presently separately on the right side. The gap sizes are indicated for the edge clusters and, inside the parenthesis, for the central cluster.

TABLE I. Renormalized couplings for case $B$: The five energy levels obtained in the first approximation are shown in the first column.

| $E$ | $T_s'$ | $T_w'$ |
|---|---|---|
| 0 | $-\frac{t}{2}$ | $\frac{t^2}{2}$ |
| $\pm\sqrt{2}$ | $\frac{t}{4}$ | $\frac{t^2}{4}$ |
| $\pm 1$ | $-\frac{t^2}{2}$ | $t^3$ |

Consequently, all the five degenerate levels will trifurcate indefinitely in the manner described in the last subsection. Figure 8 shows the level splitting pattern.

In summary, in case $B$ the Fibonacci lattice breaks into biatomic molecules and triatomic molecules, if we ignore the weaker bonds. There are five levels in the first approximation: $E=\pm T_s$ for the bonding and antibonding biatomic molecules, and $E=0,\pm\sqrt{2}T_s$ for the three normal modes of the triatomic molecules. An effective Hamiltonian can be constructed within each of the degenerate levels. But the resultant sublattices have only isolated units and double-unit molecules in a further approximation. Therefore, the previous arguments apply for the subsequent analysis. So the spectrum should consist of five main clusters, each of which trifurcates indefinitely [see Figs. 2(b) and 3(b)].

### C. Case C

Let us now consider the diagonal QC Hamiltonian (case $C$), in which the off-diagonal hopping elements are all equal to $T$, and the on-site energies $V_1, V_2$ are distributed quasiperiodically. This lattice is represented schematically in the top chain of Fig. 9.

We are interested in the situation $|V_1-V_2|\gg T$. Then, to a first approximation, we may neglect the hopping energies. The resulting energy spectrum consists of two degenerate levels $E=V_1$ and $E=V_2$, with the wave functions localized at the corresponding sites.

In the next approximation we take into account the couplings within each degenerate level due to the hopping energies. Consider, for instance, the level of $E=V_1$ corresponding to the white sites in Fig. 9. Some of the white sites are directly coupled to first order in $T$, and some of them are coupled through the dark sites to second order in $T$. A simple calculation gives the two types of coupling parameters as $T_s'=T$ and $T_w'=T^2/(V_1-V_2)$. They are arranged in the same order as in case $A$.

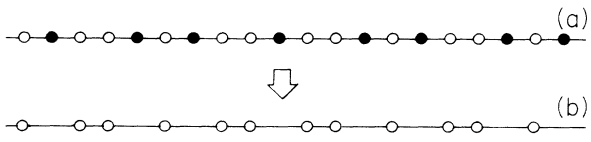


FIG. 9. Decimation procedure for the diagonal Fibonacci chain, case $C$. The two values of the on-site energies are responsible for the splitting of the energy spectra into two clusters. If we decimate one type of sites in (a), say, the dark ones, we obtain a chain of sites of equal on-site energy, but with a Fibonacci sequence of strong and weak nearest-neighbor bonds, exactly as in case $A$.

In a similar fashion the dark sites in the degenerate level $E=V_2$ are found to be coupled by the two types of nearest-neighbor bonds:

$$T_s'=\frac{T^2}{V_2-V_1}\ ,\quad T_w'=\frac{T^3}{(V_2-V_1)^2}\ . \tag{4.6}$$

Again, these bonds are distributed as in case $A$.

In summary, in case $C$ the first approximation of ignoring the bonds results in two degenerate levels. An effective Hamiltonian can be constructed for each of the levels. It can be shown that the resultant sublattices have the same structure as the Fibonacci lattice in case $A$. Thus the whole spectrum should consist of two main clusters, each of which trifurcates indefinitely [see Figs. 2(c) and 3(c)].

## V. WAVE FUNCTIONS

Our RG scheme gives a natural coding of the wave functions, by a symbolic string $p_1p_2p_3\cdots$. The $p_i$'s take values of $t$, $c$, and $b$, meaning top, central, and bottom, respectively. For instance, if the energy belongs to the central cluster, the top subcluster of the central cluster, etc., then we associate with it a string $ct\cdots$. If the string has a periodic tail, then we call the state a rational state. It is not difficult to see that for a rational state, the wave function should have a self-similar behavior. Chaotic behavior of the wave functions may appear for irrational states.

Consider the state with an energy in the center of the spectrum. This state is coded by the symbolic string $cccc\cdots$, meaning that the energy belongs to the central cluster, the central subcluster of the central cluster, and so on. According to the RG analysis, in each step of specializing into a sublattice, the wave function gets enhanced by a factor of $|T_s/T_w|$, while the average distance between the sites, $L$, gets enlarged by a factor of $\tau^3$. We therefore have

$$|\psi(L)|\sim L^{\ln|T_s/T_w|/\ln\tau^3} \tag{5.1}$$

where $L$ is a distance along the chain.

Next, we consider a state at the edge of the spectrum. This state is coded as $sss\cdots$, meaning that the energy belongs to a side cluster, a side subcluster of side cluster, and so on. In this case the average distance between the sites gets enlarged by a factor of $\tau^2$ by renormalization. Therefore,

$$|\psi(L)|\sim L^{\ln T_s/T_w/\ln\tau^2}\ . \tag{5.2}$$

These results have also been obtained using trace-map formulas.[15]

Finally, we consider a state coded by a string of mixed $s$'s and $c$'s. If the concentration of the $c$'s is $\rho_c$ and that of the $s$'s is $\rho_s$, then we should have

$$|\psi(L)| \sim L^{\ln|T_s/T_w|/\ln\tau^{(2\rho_s+3\rho_c)}} \tag{5.3}$$

This is, to our knowledge, a new result.

In order to verify the results of our RG approach further, we plotted the probability density (PD)

$$P_n = \sum_s |\psi_n^{(s)}|^2 , \tag{5.4}$$

summed over the states belonging to certain clusters and subclusters in the spectrum; $n$ represents the site position along the chain. In Fig. 10(a) the PD over the central cluster is plotted as a function of $n$. The PD is uniformly peaked on the isolated sites, which corresponds to the renormalized lattice obtained in the first step of our RG analysis for the $E=0$ level. The PD over the central subcluster of the central cluster [Fig. 10(b)] is uniformly peaked on the sites corresponding to the "superisolated" atomic states in the second step of our RG analysis. As we narrow the range of the spectrum toward the center, we see a very clear hierarchical structure in the successive PD's [Figs. 10(c) and 10(d)], exactly corresponding to what the RG suggests. On the other hand, as we plot the PD's over the top cluster [Fig. 11(a)], top subcluster of the top cluster [Fig. 11(b)], and so on [Figs. 11(c)–11(e)], we see another type of hierarchical structure corresponding to the bonding molecular states, bonding "supermolecular" states, and so on. It is important to note that lattices (a), (b), and (c) in Fig. 4 correspond, respectively, to (b), (c), and (d) in Fig. 10. Also, lattices (a), (b), and (c) in Fig. 5 correspond, respectively, to (c), (d), and (e) in

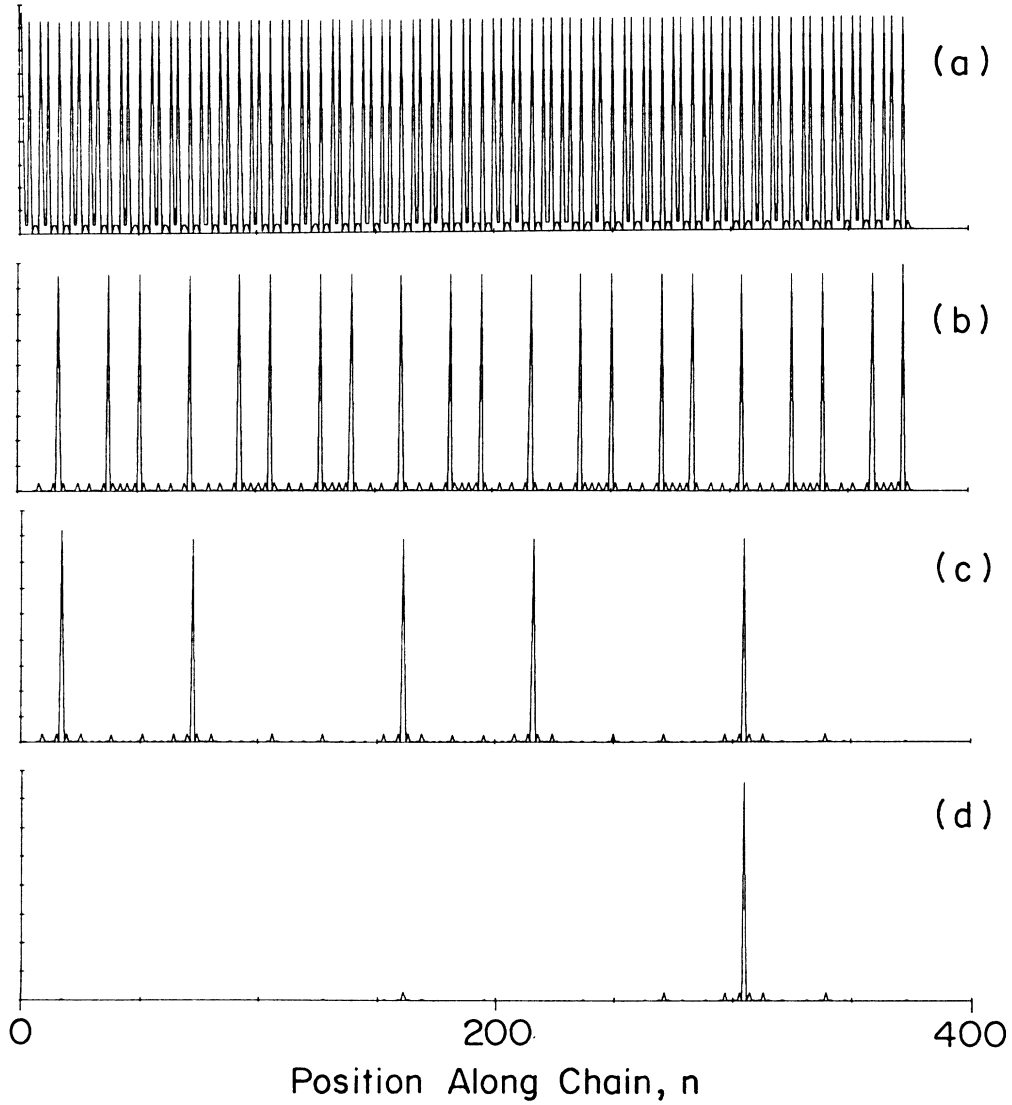


FIG. 10. Probability density $P_n = \sum_{s\in C} |\psi_n^{(s)}|^2$ of states in a central cluster $C$ vs site position $n$ along the chain. The results are for the off-diagonal case $A$. In (a), $C = C_{(1)}$, the central main cluster around $E=0$. In (b), $C = C_{(2)}$, the central subcluster of $C_{(1)}$. In (c), $C = C_{(3)}$, the central subcluster of $C_{(2)}$. And in (d), $C = C_{(4)}$, the central subcluster of $C_{(3)}$. It is remarkable that the lattices of Figs. 4(a), 4(b), and 4(c) correspond to the probability densities shown in (b), (c), and (d), respectively.

Fig. 11. The exact correspondence between them is remarkable.

## VI. LOCALIZED GAP STATES

Let $G_0(n,n';z)$ be the Green's function of a 1D tight-binding Hamiltonian $H_0$. If $H_0$ is perturbed by an additional site energy $\Delta$ at the site $a$, then the perturbed Green's function satisfies the Dyson relation

$$G(n,n';z)=G_0(n,n';z)+G_0(n,a;z)\Delta G(a,n';z) . \quad (6.1)$$

Now $G_0(a,n';z)$ can be solved by putting $n=a$ in the above equation. Then we substitute the expression of $G(a,n';z)$ back into the equation, yielding

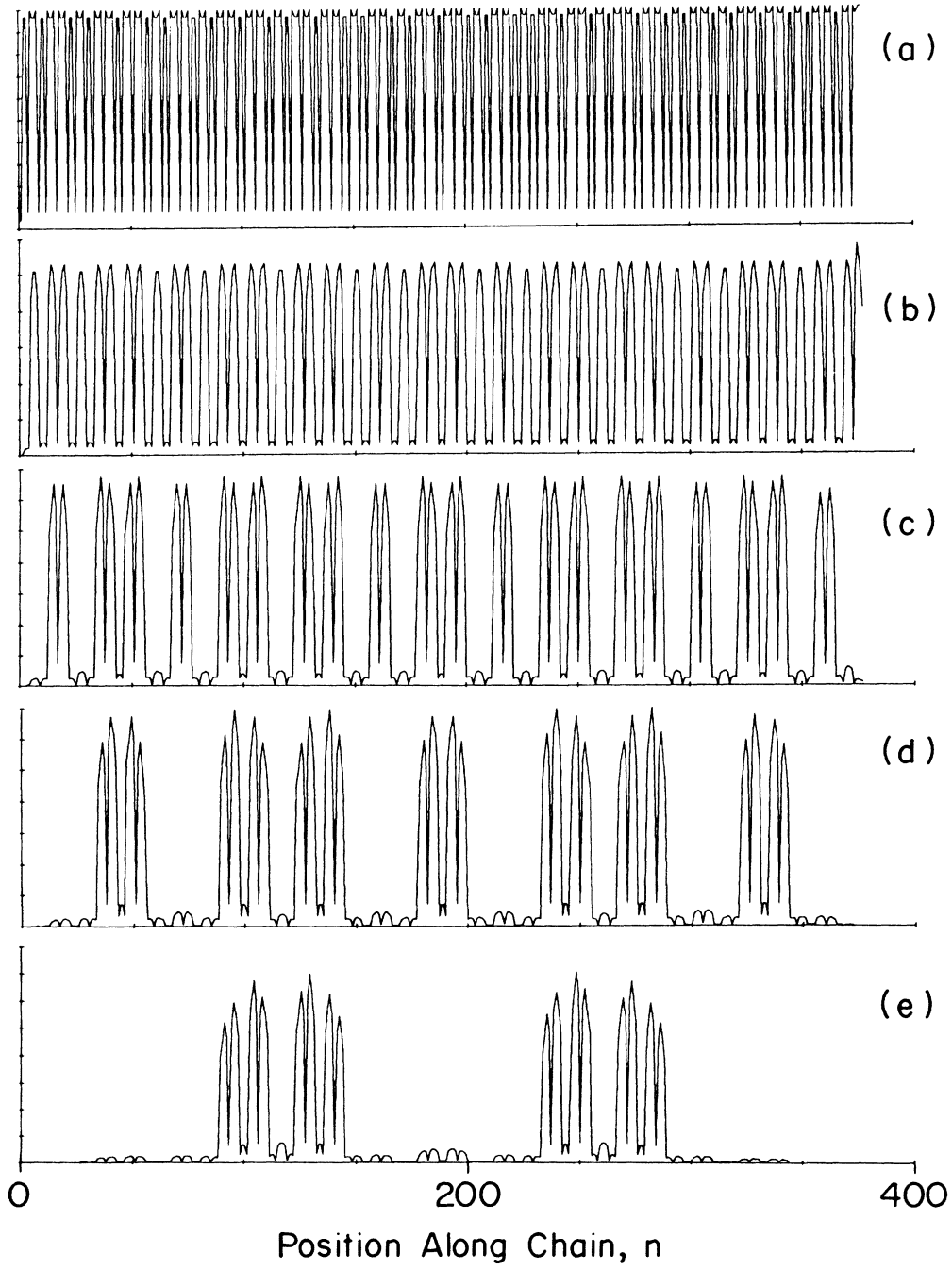


FIG. 11. Probability density $P_n=\sum_{\nu\in B}|\psi_n^{(\nu)}|^2$ of states in a top cluster $B$ vs site position $n$ along the chain. The results are for case *A*. In (a), $B=B_{(1)}$, the top main cluster of the spectrum. In (b), $B=B_{(2)}$, the top subcluster of $B_{(1)}$. In (c), $B=B_{(3)}$, the top subcluster of $B_{(2)}$. In (d), $B=B_{(4)}$, the top subcluster of $B_{(3)}$. And in (e), $B=B_{(5)}$, the top subcluster of $B_{(4)}$. It is remarkable that the lattices of Figs. 5(a), 5(b), and 5(c) correspond to the probability densities of (c), (d), and (e), respectively.

$$G(n,n';z)=G_0(n,n';z) + \frac{\Delta}{1-\Delta G_0(a,a;z)} \times G_0(n,a;z)G(a,n';z) . \quad (6.2)$$

The poles of $G$ are given by

$$G_0(a,a;z)=\frac{1}{\Delta} , \quad (6.3)$$

or

$$\sum_\alpha \frac{|\psi_\alpha(a)|^2}{z-E_\alpha}=\frac{1}{\Delta} . \quad (6.4)$$

Suppose $H_0$ represents the Hamiltonian of a quasicrystalline system. It is known that $H_0$ has, in general, a Cantor-set-like spectrum. Let us assume that $z$ lies in a gap. At the edges of the gap, the density of energy levels diverges. Thus $G_0(a,a;z)$ will be positive infinite as $z$ approaches the left edge, and it becomes negative infinite as $z$ approaches the right edge (see Fig. 12). Also, $G_0(a,a;z)$ monotonically decreases within the gap. Thus $G_0(a,a;z)$ *must* go through the values $1/\Delta$ at some point in the gap. This point is the energy of a gap state.[37,45–48] This gap state must be exponentially localized since

$$\psi_k(n)\psi_k^*(n')=\frac{1}{2\pi i}\oint_{C(z_0)} dz\, G(n,n';z) \quad (6.5)$$

$$=-\frac{G_0(n,a;z_0)G_0(a,n';z_0)}{(d/dz_0)G_0(a,a;z_0)} , \quad (6.6)$$

where $G_0(a,n;z_0)$ and $G_0(a,n';z_0)$ are exponentially small when $n$ and $n'$ are far from the site $a$, respectively.

In summary, within each gap of the original chain, there will be an impurity or gap state localized about $n=a$. Because there are an infinite number of gaps, there must also be an infinite number of impurity states.

The earlier a gap appears in the RG procedure, the more localized is the gap state in it. Consider the smallest cluster (to be coded as $p_1p_2\cdots p_n$) in the spectrum that includes this gap. This cluster corresponds to a $n$-step renormalized chain whose "sites" consist of $L_n$ sites in the original chain. Then $L_n$ is the natural length scale associated with the gap under consideration. The localization length of the gap state in it should be of order $L_n$.

The length $L_n$ can be determined from the code string $p_1p_2\cdots p_n$ according to Sec. V. Suppose the string consists of $n_s$ number of $s$'s and $n_c$ number of $c$'s, with $n_s+n_c=n$. Then we have

$$L_n=\tau^{3n_c+2n_s} . \quad (6.7)$$

Finally, let us consider the special case of $\Delta\to\infty$, then

$$G(n,n';z)=G_0(n,n';z) - \frac{G_0(n,a;z)G(a,n';z)}{G_0(a,a;z)} . \quad (6.8)$$

There are three possible behaviors of the gap states $\psi_k(n)$: (i) $\psi_k(n)$ is identically zero for $n\le a$, while it is finite for $n>a$. (ii) $\psi_k(n)$ is identically zero for $n\ge a$, but it is finite for $n<a$. (iii) $\psi_k(n)$ is finite on both sides.

In cases (i) and (iii) the impurity state is also a surface state[37] for the right part of the chain. On the other hand, case (ii) contributes nothing to the right part of the chain. Generally speaking, case (iii) is very unlikely, unless the original chain is symmetric about $n=a$. Thus, under general circumstances, there will be a fraction of these impurity states that actually correspond to the surface states of the right part of the chain.

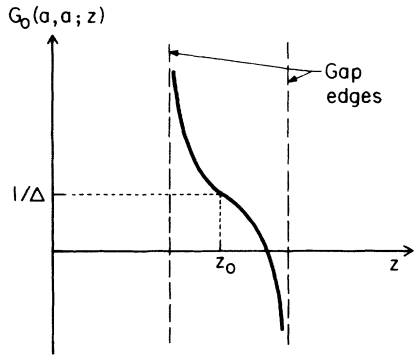


FIG. 12. Unperturbed Green's function vs energy $z$ in a gap of the spectrum. At the edges of the gap, the density of energy levels diverges, so that $G_0$ also diverges there. The energy $z_0$ is that of an exponentially localized gap state.

## VII. CONCLUSIONS

We have presented a RG analysis on the spectral and wave-function properties of quasicrystalline and hierarchical chains. We have shown how the trifurcating or bifurcating structure of the spectrum is directly related to the self-similarity of the underlying lattices. The RG scheme also gives a natural coding of the wave functions according to their positions in the spectrum, from which the scaling structure of the wave functions is easily characterized.

Our RG theory is based on a novel real-space decimation procedure. The usual decimation technique is to eliminate all but a chosen subset of sites, resulting in renormalized coupling parameters which are energy dependent. The energy dependence makes the subsequent analysis very difficult, and numerical computations are indispensable. In our case the decimation is through a block diagonalization of the original Hamiltonian. Each block represents a decimated chain with renormalized coupling parameters that are energy independent. The trace-map technique is an alternative powerful tool to study the spectral and wave-function properties on lattices with inflation symmetry. Unfortunately, this method has only given analytical results at a few points in the spectrum.

The global multifractal analysis of the spectrum has been carried out by Zheng,[14] using the analytical formulas in the present RG theory. His result agrees with the numerical results of Ref. 15 asymptotically as $T_w/T_s\to 0$. Such an analysis has so far not been done for the wave

functions using the analytical tools of the present RG theory.

We have so far only studied four cases using the RG theory. It is also possible to apply the method to other 1D systems. One point should be emphasized. In the present work we initially constructed a RG theory, which is then numerically verified by plotting the probability density over the clusters, subclusters, and so on. For a general quasiperiodic system, it might not be easy to find a RG theory beforehand. Thus, in a numerical approach, we suggest that one should find not just the energy spectrum, but also the probability density of the clusters, subclusters, and so on. There should be an intimate relationship between the behavior of the densities and the energy ranges of the clusters. By doing so, one can gain deeper insight into the problem. With luck, one may even be able to find a RG theory afterwards. The probability densities may also be plotted in momentum space, which could be useful for nearly free quasiperiodic systems. In this case the wave function peaks in momentum space, but not in real space.

The possibility of applying the present RG theory to higher-dimensional lattices has not been explored sufficiently; however, we estimate it to be unlikely. One major difficulty is the proliferation of more and more coupling parameters under renormalization. This is an unfortunate feature shared by other RG theories.

## ACKNOWLEDGMENTS

This research was supported by the Physics Department of the University of Michigan and the University of California, Santa Barbara, by the U.S. Office of Naval Research Grant No. N00014-84-K-0548, U.S. Department of Energy Grant No. DE84ER45108, and National Science Foundation Grants No. DMR-87-03434 and No. PHY-89-04035, supplemented by funds from U.S. National Aeronautics and Space Administration NASA.

## APPENDIX A: DEGENERATE PERTURBATION FORMALISM

Our goal now is to obtain a generalized Wigner-Brillouin perturbative expansion appropriate to a degenerate level. Let us denote by $H_0$ the Hamiltonian in the absence of weak bonds, and by $H_1$ the perturbation to $H_0$ due to the weak bonds. Let $Q$ and $P=1-Q$ denote the projection operators onto and off the subspace of a given degenerate level of $H_0$, respectively. By definition, $Q$ and $P$ commute with $H_0$ and with each other, and they satisfy $Q^2=Q$ and $P^2=P$. By acting with $Q$ and $P$ on our eigenvalue equation

$$(E-H_0)|\psi\rangle=H_1|\psi\rangle \ , \tag{A1}$$

we obtain two coupled equations for $Q|\psi\rangle$ and $P|\psi\rangle$ as

$$(E-H_0)Q|\psi\rangle=QH_1Q\cdot Q|\psi\rangle+QH_1P\cdot P|\psi\rangle \ , \tag{A2}$$

$$(E-H_0)P|\psi\rangle=PH_1Q\cdot Q|\psi\rangle+PH_1P\cdot P|\psi\rangle \ . \tag{A3}$$

From (A3) we have

$$P|\psi\rangle=\frac{1}{E-H_0-PH_1P}PH_1Q\cdot Q|\psi\rangle \ . \tag{A4}$$

We then substitute it into (A2) to obtain an equation for $Q|\psi\rangle$ only:

$$(E-H_0)Q|\psi\rangle=QH_1Q\cdot Q|\psi\rangle+QH_1P\frac{1}{E-H_0-PH_1P}PH_1Q\cdot Q|\psi\rangle \ . \tag{A5}$$

Thus the effective Hamiltonian for the degenerate level is

$$H_{\text{eff}}=H_0+QH_1Q+QH_1P\frac{1}{E-H_0-PH_1P}PH_1Q \ . \tag{A6}$$

The previous expression may be further expanded in powers of $H_1$ as

$$H_{\text{eff}}=QH_0Q+QH_1Q+QH_1P\frac{1}{E-H_0}PH_1Q+QH_1P\frac{1}{E-H_0}PH_1P\frac{1}{E-H_0}PH_1Q+\cdots \ , \tag{A7}$$

which generalizes the Brillouin-Wigner perturbative expansion. In practice, we only need to keep the leading nonzero terms in this expansion.

## APPENDIX B: COMPUTATION OF THE RENORMALIZED COUPLINGS

Our goal here is to calculate in detail the effective couplings of a renormalized chain. Let us consider, for instance, the four-site chain shown in Fig. 13. It consists of two strongly coupled pairs of sites separated by a weak coupling given by $T_w$.

The original basis $\{|1\rangle,|2\rangle,|3\rangle,|4\rangle\}$ consists of four

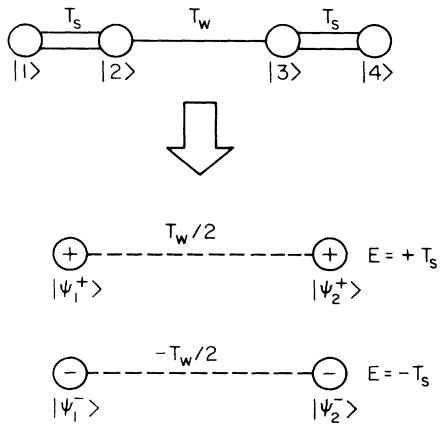


FIG. 13. Computation of the renormalized couplings for the top chain with four sites. The weak bonds have a negligible effect in mixing the bonding ($E=T_s$) and antibonding ($E=-T_s$) levels. However, they can have a big effect in splitting the degenerate levels.

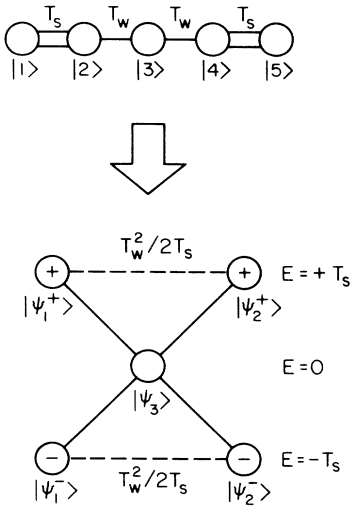


FIG. 14. Computation of the renormalized couplings for the top chain with five sites. The corresponding bonding ($E=T_s$) and antibonding ($E=-T_s$) degenerate levels, and the only nondegenerate ($E=0$) level, are shown. The effect of the weak couplings is to lift the degeneracy of the antibonding states. The effective coupling among states that belong to the same degenerate subspace is indicated.

normalized site states. The Hamiltonian has one term $H_0$ due to the presence of the strong coupling $T_s$ and a perturbation $H_1$ due to the weak coupling $T_w$. The only nonzero matrix elements of $H_0$ are given by

$$\langle 1|H_0|2\rangle=\langle 2|H_0|1\rangle=\langle 3|H_0|4\rangle=\langle 4|H_0|3\rangle =+T_s \ , \tag{B1}$$

while the only nonzero matrix elements of $H_1$ are $\langle 2|H_1|3\rangle=\langle 3|H_1|2\rangle=+T_w$. $H_0$ is diagonalized in the following basis:

$$|\psi_1^{\pm}\rangle=\frac{1}{\sqrt{2}}(|1\rangle\pm|2\rangle) \ , \qquad |\psi_2^{\pm}\rangle=\frac{1}{\sqrt{2}}(|3\rangle\pm|4\rangle) \ . \tag{B2}$$

The two bonding states $|\psi_1^+\rangle, |\psi_2^+\rangle$ are degenerate and have the energy $T_s$, while the antibonding states are also degenerate with energy $-T_s$.

Because of the large gap, $H_1$ has a negligible effect in mixing the bonding and antibonding levels. However, $H_1$ can have a big effect in splitting the degenerate levels.

Since

$$H_1|\psi_1^{\pm}\rangle=\pm\frac{T_w}{\sqrt{2}}|3\rangle \ , \tag{B3}$$

and

$$H_1|\psi_2^{\pm}\rangle=\frac{T_w}{\sqrt{2}}|2\rangle \ , \tag{B4}$$

the effect of $H_1$ on the bonding level is given by

$$\langle\psi_1^+|H|\psi_2^+\rangle=\frac{T_w}{2} \ , \tag{B5}$$

and its effect on the antibonding level is given by

$$\langle\psi_1^-|H|\psi_2^-\rangle=-\frac{T_w}{2} \ . \tag{B6}$$

These considerations have taken into account the leading two terms in $H_{\text{eff}}$ given in Appendix A. Higher-order terms are negligible.

Next, we will consider a more complicated case, in which the next-higher-order term of $H_{\text{eff}}$ must be kept. Figure 14 shows a five-site chain, with two strong bonds and two weak ones.

The unperturbed Hamiltonian $H_0$, due to the strong bonds, is diagonalized in the following basis:

$$|\psi_1^{\pm}\rangle=\frac{1}{\sqrt{2}}(|1\rangle\pm|2\rangle) \ , \qquad |\psi_2^{\pm}\rangle=\frac{1}{\sqrt{2}}(|4\rangle\pm|5\rangle) \ , \quad |\psi_3\rangle=|3\rangle \ . \tag{B7}$$

Clearly, $H_0|\psi_i^{\pm}\rangle=\pm T_s|\psi_i^{\pm}\rangle$ $(i=1,2)$ and $H_0|\psi_3\rangle=0$.

We wish to obtain the coupling between the two degenerate bonding states $|\psi_1^+\rangle$ and $|\psi_2^+\rangle$. The first term in perturbation theory vanishes, i.e., $QH_1Q=0$. The second-order term in $H_{\text{eff}}$ provides the leading nonzero contribution to the coupling

$$\langle\psi_2^+|H_{\text{eff}}|\psi_1^+\rangle=\left\langle\psi_2^+\left|H_1P\frac{1}{E-H_0}PH_1\right|\psi_1^+\right\rangle \ . \tag{B8}$$

In this expression we have $E=T_s$, and

$$P=|\psi_1^-\rangle\langle\psi_1^-|+|\psi_2^-\rangle\langle\psi_2^-|+|\psi_3\rangle\langle\psi_3| \ . \tag{B9}$$

The only nonzero term of (B8) is

$$\langle\psi_2^+|H_1|\psi_3\rangle\left\langle\psi_3\left|\frac{1}{T_s-H_0}\right|\psi_3\right\rangle\langle|\psi_3|H_1|\psi_1^+\rangle \ , \tag{B10}$$

which gives

$$\langle\psi_2^+|H_{\text{eff}}|\psi_1^+\rangle=\frac{T_w}{\sqrt{2}}\frac{1}{T_s}\frac{T_w}{\sqrt{2}}=\frac{1}{2}\frac{T_w^2}{T_s} \ . \tag{B11}$$

Similarly, the coupling between the two antibonding states is given by

$$\langle\psi_2^-|H_{\text{eff}}|\psi_1^-\rangle=\left\langle\psi_2^-\left|H_1P\frac{1}{E-H_0}PH_1\right|\psi_1^-\right\rangle \ , \tag{B12}$$

where now $E=-T_s$, and

$$P=|\psi_1^+\rangle\langle\psi_1^+|+|\psi_2^+\rangle\langle\psi_2^+|+|\psi_3\rangle\langle\psi_3| \ . \tag{B13}$$

The only nonzero term in (B12) is

$$\langle\psi_2^-|H_1|\psi_3\rangle\left\langle\psi_3\left|\frac{1}{E-H_0}\right|\psi_3\right\rangle\langle\psi_3|H_1|\psi_1^-\rangle \ , \tag{B14}$$

which gives

$$\langle\psi_2^-|H_{\text{eff}}|\psi_1^-\rangle=\frac{T_w}{\sqrt{2}}\frac{1}{-T_s}\frac{-T_w}{\sqrt{2}}=\frac{1}{2}\frac{T_w^2}{T_s} \ . \tag{B15}$$

*Present address.
[1]R. Merlin, K. Bajema, R. Clarke, F.-Y. Juang, and P. K. Bhattacharaya, Phys. Rev. Lett. **55**, 1768 (1985).
[2]J. Todd, R. Merlin, R. Clarke, K. M. Mohanty, and J. D. Axe, Phys. Rev. Lett. **57**, 1157 (1986); **59**, 2237 (1987).
[3]K. Bajema and R. Merlin, Phys. Rev. B **36**, 4451 (1987).
[4]S. Tamura and J. Wolfe, Phys. Rev. B **36**, 3491 (1987); **38**, 5610 (1988); D. C. Hurley, S. Tamura, J. P. Wolfe, K. Ploog, and J. Nagle, *ibid.* **37**, 8829 (1988).
[5]S. Tamura and F. Nori, Phys. Rev. B **40**, 9790 (1989); **41**, 7941 (1990).
[6]See, for instance, *Aperiodicity and Order,* edited by M. V. Jaric (Academic, Boston, 1988).
[7]A. Behrooz *et al.*, Phys. Rev. B **35**, 8396 (1987); K. Springer and D. Van Harlingen, *ibid.* **36**, 7273 (1987); Y. Y. Wang *et al.*, Jpn. J. Appl. Phys. **26**, Suppl. **26-3**, 1415 (1987).
[8]F. Nori, Q. Niu, E. Fradkin, and S.-J. Chang, Phys. Rev. B **36**, 8338 (1987).
[9]Q. Niu and F. Nori, Phys. Rev. B **39**, 2134 (1989).
[10]R. Merlin, IEEE J. Quantum Electron. **QE-24**, 1791 (1988).
[11]J. B. Sokoloff, Phys. Rep. **126**, 189 (1985).
[12]Q. Niu and F. Nori, Phys. Rev. Lett. **57**, 2057 (1986).
[13]A. Garg, Phys. Rev. B **37**, 10003 (1988), in particular Appendix B, p. 10018.
[14]W. M. Zheng, Phys. Rev. A **35**, 1467 (1987).
[15]M. Kohmoto, B. Sutherland, and C. Tang, Phys. Rev. B **35**, 1020 (1987).
[16]M. Kohmoto, L. P. Kadanoff, and C. Tang, Phys. Rev. Lett. **50**, 1870 (1983).
[17]S. Ostlund, R. Pandit, D. Rand, H. J. Schellnhuber, and E. D. Siggia, Phys. Rev. Lett. **50**, 1873 (1983).
[18]M. Kohmoto and J. Banavar, Phys. Rev. B **34**, 563 (1986).
[19]M. Kohmoto, B. Sutherland, and K. Iguchi, Phys. Rev. Lett. **58**, 2436 (1987).
[20]B. Sutherland, Phys. Rev. Lett. **57**, 770 (1986).
[21]Y. Liu and R. Riklund, Phys. Rev. B **35**, 6034 (1987).
[22]J. M. Luck and D. Petritis, J. Stat. Phys. **42**, 289 (1986).
[23]S. Das Sarma, A. Kobayashi, and R. E. Prange, Phys. Rev. Lett. **56**, 1280 (1986); Phys. Rev. B **34**, 5309 (1986).
[24]S. Das Sarma and X. C. Xie, Phys. Rev. B **37**, 1097 (1988).
[25]G. Gumbs and M. K. Ali, Phys. Rev. Lett. **60**, 1081 (1988).
[26]M. Kolař and M. K. Ali, Phys. Rev. A **39**, 6538 (1989); Phys. Rev. B **39**, 426 (1989); *ibid.* **41**, 7108 (1990).
[27]M. Kolař, M. K. Ali, and F. Nori, Phys. Rev. B (to be published).
[28]M. Kolař and F. Nori, Phys. Rev. B **42**, 1062 (1990).
[29]M. Holzer, Phys. Rev. B **38**, 1709 (1989); **38**, 5756 (1989).
[30]J. A. Vergés, J. Brey, E. Louis, and C. Tejedor, Phys. Rev. B **35**, 5270 (1987).
[31]D. J. Thouless and Q. Niu, J. Phys. A **16**, 1911 (1983).
[32]J. P. Lu, T. Odagaki, and J. L. Birman, Phys. Rev. B **33**, 4809 (1986).
[33]P. A. Kalugin, A. Yu. Kitaev, and L. S. Levitov, Zh. Eksp. Teor. Fiz. **91**, 692 (1986) [Sov. Phys.—JETP **64**, 410 (1987)].
[34]L. S. Levitov (unpublished).
[35]J. A. Ashraff and R. B. Stinchcombe, Phys. Rev. B **37**, 5723 (1988).
[36]A. Chakrabarti, S. N. Karmakar, and R. K. Moitra, Phys. Rev. B **39**, 9730 (1989).
[37]F. Nori and J. P. Rodriguez, Phys. Rev. B **34**, 2207 (1986).
[38]K. Machida and M. Fujita, Phys. Rev. B **34**, 7367 (1986); Solid State Commun. **59**, 61 (1986).
[39]R. Riklund, M. Severin, and Y. Liu, Int. J. Mod. Phys. B **1**, 121 (1987).
[40]C. Evangelou, J. Phys. C **20**, L295 (1987).
[41]R. Rammal, G. Tolouse, and M. A. Virasoro, Rev. Mod. Phys. **58**, 765 (1986).
[42]H. E. Roman, Phys. Rev. B **36**, 7173 (1987); **37**, 1399 (1988).
[43]H. A. Cecatto, W. P. Keirstead, and B. Huberman, Phys. Rev. A **36**, 5509 (1987); J. Stat. Phys. **53**, 733 (1988).
[44]T. Schneider, D. Wurtz, A. Politi, and M. Zannetti, Phys. Rev. B **36**, 1789 (1987); **39**, 7829 (1989).
[45]X. C. Xie and S. Das Sarma, Phys. Rev. Lett. **60**, 1585 (1988); V. Kumar and G. Ananthakrishna, *ibid.* **59**, 1476 (1987); **60**, 1586 (1988).
[46]F. Laruelle and B. Etienne, Phys. Rev. B **37**, 4816 (1988).
[47]R. B. Capaz, Belita Koiller, and S. L. A. de Queiroz, Phys. Rev. B **43**, 6402 (1991).
[48]K. W.-K. Shung, L. M. Sander, and R. Merlin, Phys. Rev. Lett. **61**, 455 (1988).